Data Mine

A High-Precision Earthquake Catalog for Nevada

Daniel T. Trugman*[1]

Abstract

The state of Nevada is home to one of the most seismically active regions in the world, with crustal deformation associated with the Walker Lane transitioning into Basin and Range tectonics as one traverses from west to east across the state. Despite hosting numerous prominent earthquake sequences over the past century and beyond, at present, there exists no unified research-quality earthquake catalog for the state and its surrounding region. Here, we present a newly compiled, high-precision catalog of more than 180,000 earthquakes occurring around Nevada from 2008 to 2023. The data processing workflow to create this catalog includes an absolute location step that accounts for topography and 3D variations in subsurface wavespeed, and a relative relocation step that refines event positions using differential times measured from waveform cross-correlation. We also provide an update to the local magnitude scale that better accounts for the observed distance attenuation of waveform amplitudes as well as local site effects. We describe some fundamental insights that can be derived from the new catalog, including regional variations in event depth distributions and sequence clustering statistics, and publish the catalog to the wider community to facilitate future research efforts.

Cite this article as Trugman, D. T. (2024). A High-Precision Earthquake Catalog for Nevada, *Seismol. Res. Lett.* **XX**, 1–9, doi: 10.1785/0220240106.

Introduction

Poised between Walker Lane along its western border and the Basin and Range to the east, Nevada has a long and rich history of earthquake activity encompassing the historical record and beyond. The early- and mid-twentieth century featured numerous prominent earthquakes in west-central Nevada (Ryall, 1977), including the 1915 **M** 7.3 Pleasant Valley earthquake (Jones, 1915), the 1932 **M** 7.1 Cedar Mountain earthquake (Gianella and Callaghan, 1934), the 1954 **M** 6.6 Rainbow Mountain earthquake and **M** 6.7 Stillwater earthquake sequence (Tocher, 1956), and the 1954 **M** 7.2 Fairview Peak earthquake and **M** 7.1 Dixie Valley earthquake sequence (Slemmons, 1957). More recently, earthquake sequences including 2008 **M** 5.0 Mogul (Ruhl *et al.*, 2016), 2008 **M** 6.0 Wells (Mendoza and Hartzell, 2009), 2016 **M** 5.4–5.6 Nine Mile Ranch (Hatch-Ibarra *et al.*, 2022), 2020 **M** 6.5 Monte Cristo (Ruhl *et al.*, 2021), and 2023 **M** 6.0 Antelope Valley (Trugman, Brune, *et al.*, 2023) were widely felt and are representative of the ongoing crustal deformation that characterizes this tectonically complex region.

Despite this remarkable history of earthquake activity, no research-grade earthquake catalog currently exists for the state of Nevada and the surrounding region. The Nevada Seismological Laboratory (NSL) operates a Tier 1 Regional Seismic Network as part of the Advanced National Seismic System and is tasked with monitoring earthquake activity in and around the state, reporting phase arrival and earthquake catalog information to the U.S. Geological Survey's (USGS) Comprehensive Catalog (ComCat). This information, although essential for real-time monitoring and hazard mitigation purposes, is not of sufficient precision for many research purposes that hinge on location accuracy and uniformity in data processing. In contrast, the neighboring state of California has two well-established research catalogs covering the northern and southern parts of the state (Waldhauser and Schaff, 2008; Hauksson *et al.*, 2012) that complement the operational monitoring catalogs reported in near-real time to ComCat. Both research catalogs in California refine initial hypocentral locations through double-difference algorithms (Waldhauser and Ellsworth, 2000; Trugman and Shearer, 2017) that leverage differential travel times from pairs of events measured via waveform cross-correlation.

The purpose of this article is to develop and describe a high-precision earthquake catalog for Nevada and the surrounding region. The workflow applied in this study takes advantage of recent advances in earthquake location technology, including regional-scale 3D velocity models, topographic effects, which

1. Nevada Seismological Laboratory, Nevada Geosciences, University of Nevada, Reno, Reno, Nevada, U.S.A., https://orcid.org/0000-0002-9296-4223 (DTT)

*Corresponding author: dtrugman@unr.edu

© Seismological Society of America

Downloaded from http://pubs.geoscienceworld.org/ssa/srl/article-pdf/doi/10.1785/0220240106/6527156/srl-2024106.1.pdf
by University of Nevada Reno, dtrugman

are particularly important for the mountainous regions along the California–Nevada border, and cluster-based double-difference algorithms that can be applied at scale to large differential time datasets. As part of this effort, we also provide an update to the local magnitude scale that more reliably accounts for the effects of ray-path attenuation and site effects on the waveform amplitude data used to estimate local magnitude. The refined earthquake catalog covers the modern era of earthquake monitoring in Nevada, 2008–2023, a time period in which station coverage improved markedly and broadband seismometers and strong-motion instrumentation became standard within NSL operations. We describe some basic features of seismicity during this time period that are revealed by the new catalog and anticipate that future research will uncover a great deal more through additional analyses of the newly published catalog.

Data and Methods

Compiling a new earthquake catalog is simple in concept but in practice requires a diverse range of datasets and techniques to synthesize the final product. Below we describe the different datasets and methodologies deployed to create a new high-precision catalog for Nevada. Individual tasks are broken up into subsections for reader clarity.

Data overview

To begin, we consider all local earthquakes (excluding blasts and explosions) detected by NSL analysts during 2008–2023 and falling within the geographical boundaries of longitude: [−121.3°, −113.5°] and latitude: [35.0°, 42.1°]. We compile phase arrival times determined by NSL analysts for each event from an internal database; these arrival times are also published to ComCat for public use. We then extract from the NSL archive waveform segments associated with each earthquake recorded at stations within 200 km epicentral distance. At each station, we window the waveforms between 5 s before the theoretical *P*-wave arrival and 30 s after the theoretical *S*-wave arrival time. Waveforms are extracted from all available stations within the 200 km search radius, regardless of whether they have a listed phase arrival, because in this workflow the waveforms are only used in waveform cross-correlation measurements that do not require absolute arrival-time information.

Absolute location technique

The operational catalog published in near-real time by the NSL uses a simplified location algorithm that neglects 3D variations in subsurface wavespeed and surface topography. In our workflow, we use the recently published California and Nevada Adjoint Simulations (CANVAS) regional velocity model (Doody *et al.*, 2023) in tandem with station elevation information to provide more accurate absolute location estimates for events in our study region. To achieve this, we use the NonLinLoc algorithm (Lomax *et al.*, 2000, 2014), which combines an Eikonal solver for ray tracing through 3D velocity models with a probabilistic search algorithm to determine event hypocentral location estimates and uncertainties.

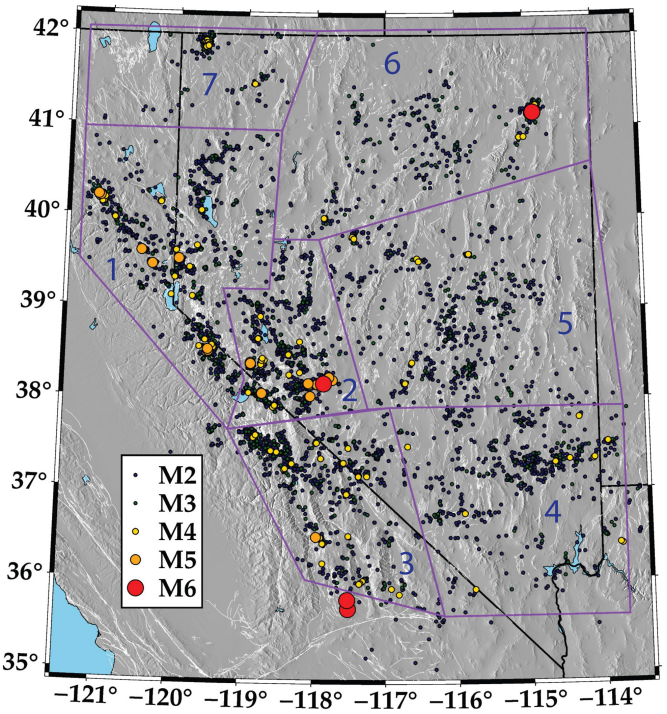

Figure 1. Overview map of seismicity within the study region. The seven regional polygons for location analysis are marked in purple. The U.S. Geological Survey (USGS) Quaternary faults are marked as thin white lines. The color version of this figure is available only in the electronic edition.

Because of the size of our study region, we divided it into seven smaller polygons featuring coherent clusters of seismicity (Fig. 1). Polygons were selected to form coherent regions of seismicity without truncating significant clusters. Each polygon overlaps by 5 km, which helps to mitigate potential artifacts from processing earthquakes near the edge of each polygon boundary that would otherwise be cut off from their cross-correlation neighbors. The purpose of the subdivision into polygons is twofold: (1) to ensure that the map projection used in the 3D location algorithm remains locally accurate to good approximation and (2) to allow for the 3D travel-time grids associated with each station and phase to fit into computer memory during the location process. Within each polygon, we locate events using the Weighted Equal Differential Time module of NonLinLoc applied to all analyst-defined phases within 150 km of the source in areas of dense station coverage (polygons 1–4), extending to 200 km in more remote regions (polygons 5–7). We run NonLinLoc once to determine initial locations and estimates of station delays not captured by the CANVAS velocity model, and then run it a second time to refine these locations accounting for these station delays.

Downloaded from http://pubs.geoscienceworld.org/ssa/srl/article-pdf/doi/10.1785/0220240106/6527156/srl-2024106.1.pdf
by University of Nevada Reno, dtrugman

Relative relocation technique

To refine the precision of the absolute event locations, we measure differential travel times from pairs of nearby earthquakes recorded at a set of common stations and input the resulting differential time dataset into the GrowClust3D.jl (Trugman *et al.*, 2022) relative relocation software package. For each earthquake, we identify neighboring events for cross-correlation within a 5 km search radius, up to a maximum of 1000 nearest neighbors. For each event pair, we then cross-correlate waveforms for time windows corresponding to the direct *P*- and *S*-wave arrival windows separately, with the *P*-wave window starting 0.2 s before the theoretical arrival and lasting 1.5 s in length, and the *S*-wave window starting 0.2 s before the theoretical arrival and lasting 2.5 s in length. All waveforms are band-pass filtered into the decade from 1.2 to 12 Hz—a frequency band selected to maximize signal-to-noise on broadband recordings of local earthquakes. Differential travel times are measured from the peak of the cross-correlation function, fit with a spline interpolant of precision 0.001 s. For quality-control purposes, we discard all measurements with peak values less than 0.65 or sidelobes within 0.1 units of the peak, the latter to mitigate cycle-skipping effects.

We input into GrowClust3D.jl the subset of quality-controlled differential travel times corresponding to all event pairs with at least eight differential time measurements of correlation value 0.65 or higher. For consistency, we use the same travel-time grids, map projection, and topographic information in the relative relocation algorithm of GrowClust3D.jl as was used by NonLinLoc to obtain absolute locations. Each polygon is relocated separately, and the results are then merged to create the final relocated event catalog.

A revised magnitude scale

The NSL reports local magnitude (M_L) estimates for most earthquakes derived from measurements of Wood–Anderson equivalent displacement amplitudes, corrected for distance (Richter, 1935). Although this practice is common to most regional seismic networks, at present, the NSL workflow is somewhat outdated, using a southern-California-specific, piecewise-constant distance correction function (Richter, 1958) instead of a smooth curve, and neglecting local site effects, which are commonly mitigated through station correction terms (Uhrhammer *et al.*, 2011). With these limitations in mind, we seek to develop a new magnitude scale for the state that better captures known physical processes controlling waveform amplitude measurements while still retaining a parsimonious functional form that could be used in real-time operations. To this end, we seek to resolve a local magnitude relation of the form

$$M_{ij} = \log_{10} A_{ij} + c_0 + c_1 \log_{10} R_{ij} + c_2 R_{ij} + dS_j, \quad (1)$$

in which A_{ij} is the amplitude of event i recorded at station j, R_{ij} is the epicentral distance from event i to station j, and dS_j is a station correction term, and c_0, c_1, and c_2 are regression coefficients. Conceptually, c_1 and c_2 represent the effects of geometric spreading and path attenuation on waveform amplitude, respectively, whereas c_0 is a definitional constant that ties the magnitude scale to the chosen amplitude at a reference distance.

To solve for the unknowns in equation (1), we initially set all station terms to zero and examine pairwise differences in amplitude for recordings of individual events at different distances. Doing so has the effect of canceling out the magnitude on the left side of equation (1), which is a priori unknown. Consider a single event of unknown magnitude, recorded at two stations indexed 1 and 2. If we subtract instances of equation (1) for each station, we obtain a differential formula of the form

$$\log_{10}(A_2/A_1) = c_1 \log_{10}(R_1/R_2) + c_2(R_1 - R_2). \quad (2)$$

By collecting many such within-event pairs of amplitudes and distances, we can set up a linear regression problem to solve for the unknown coefficients c_1 and c_2 (c_0 can be defined rather than estimated, consistent with the original Richter definition of the magnitude scale).

To synthesize a dataset for regression analysis, we divide events into 21 magnitude bins of 0.1 unit increments from 1.5 to 3.5 (using the original NSL magnitude scale) and randomly sample 10,000 amplitude pairs from earthquakes within each bin. This approach balances the dataset across different event sizes, ensuring the regression fit is not dominated by the smallest earthquakes (which are most frequent in number) and removing both the smallest and largest events from consideration, for which amplitudes may be contaminated by noise or clipping, respectively. The coefficient estimates —$c_0 = 0.309939$, $c_1 = 1.231613$, and $c_2 = 0.002268$—are similar to values obtained in California (Jennings and Kanamori, 1983) and align well with the initial amplitude decay function (Fig. 2a), except at the closest distances where the piecewise constant formulation is most invalid in its accounting for the effects of geometric spreading. With the new regression coefficients, we can then use the within-event residuals, aggregated across events, to estimate station correction terms. The correction terms for each station are plotted in map view (Fig. 2b), with stations with persistently high- or low-magnitude estimates (positive or negative station terms) shown in red and blue colors, respectively. The spatial patterns of these station terms are only coherent over the shortest length scales, suggesting that they capture local site effects rather than path-averaged trends in attenuation.

Results

The new, high-precision catalog of Nevada seismicity from 2008 to 2023 includes 183,002 events relocated by NonLinLoc using a 3D velocity model, of which a subset of 103,976 (~57%) are additionally waveform-relocated with

Downloaded from http://pubs.geoscienceworld.org/ssa/srl/article-pdf/doi/10.1785/0220240106/6527156/srl-2024106.1.pdf
by University of Nevada Reno, dtrugman

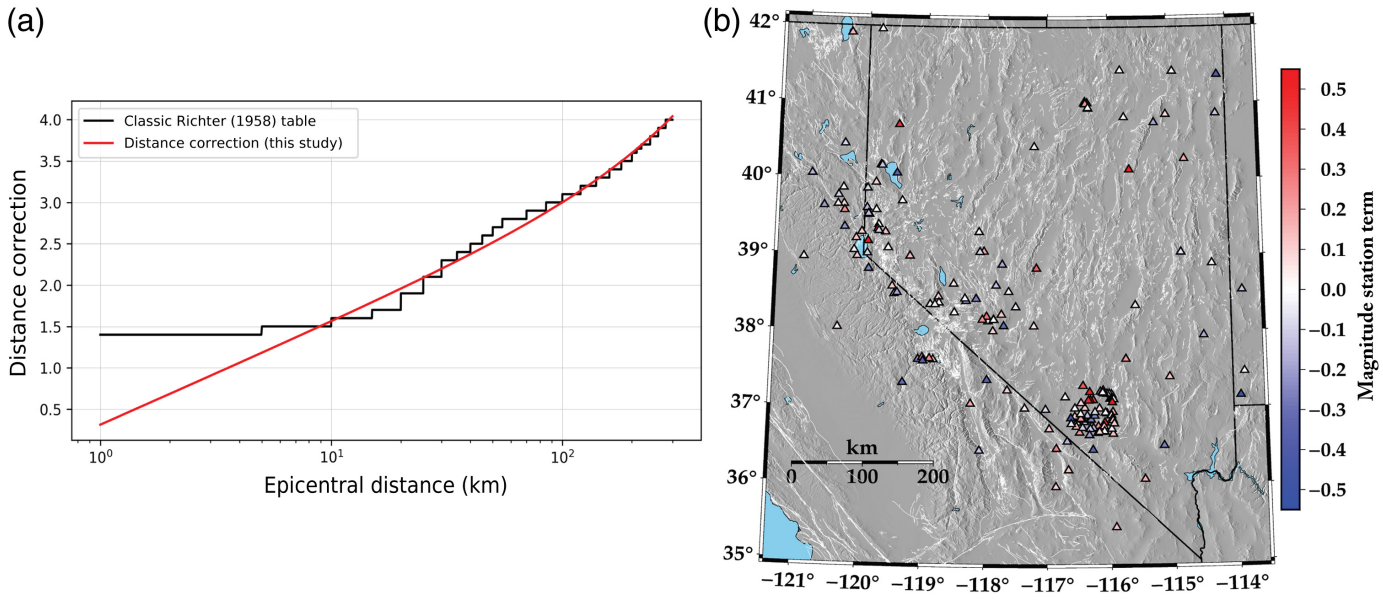

Figure 2. Revisions to the local magnitude scale. (a) Comparison of the piecewise-constant distance correction function currently used in the Nevada Seismological Laboratory (NSL) network operations (black) with the continuous distance correction function developed in this study (red). (b) Station correction terms plotted in map view, with red or blue colors indicating stations with consistently high- or low-magnitude estimates, respectively. The color version of this figure is available only in the electronic edition.

GrowClust3D.jl. Changes to the absolute locations of the earthquake hypocenters vary regionally and from event to event. Still, median shift values are ∼1 km laterally and in the 1–2 km range vertically, with more variance in the vertical shifts. Unlike the NSL catalog reported to ComCat, all event depths in the relocated catalog are reported relative to 0 km at mean sea level. Although relatively short in duration (16 yr), the catalog encompasses several prominent sequences, including the 2008 Mogul and 2014 Spanish Springs sequences near Reno, the 2008 Wells sequence in northeast Nevada, the 2014 Sheldon sequence in northwest Nevada, and the 2016 Nine Mile Ranch, 2020 Monte Cristo, and 2021 Antelope Valley sequences in the Central Walker Lane near the California–Nevada border (Fig. 3). The catalog is also exceptionally detailed in southern Nevada, where despite a paucity of large earthquakes, the dense station coverage associated with monitoring at the Nevada National Security Site (NNSS) enhances detection and location capabilities.

One advantage of using a 3D velocity model for earthquake locations is the improved resolution and consistency of hypocentral depth estimates across the study region. We quantify local and regional trends in depth distribution by computing the 95th percentile depths (D95) within spatial grid cells of 10 km radius spanning the study region (Fig. 4). For this analysis, we only include grid cells containing at least 30 events to ensure an adequate sample size for statistical analysis. The

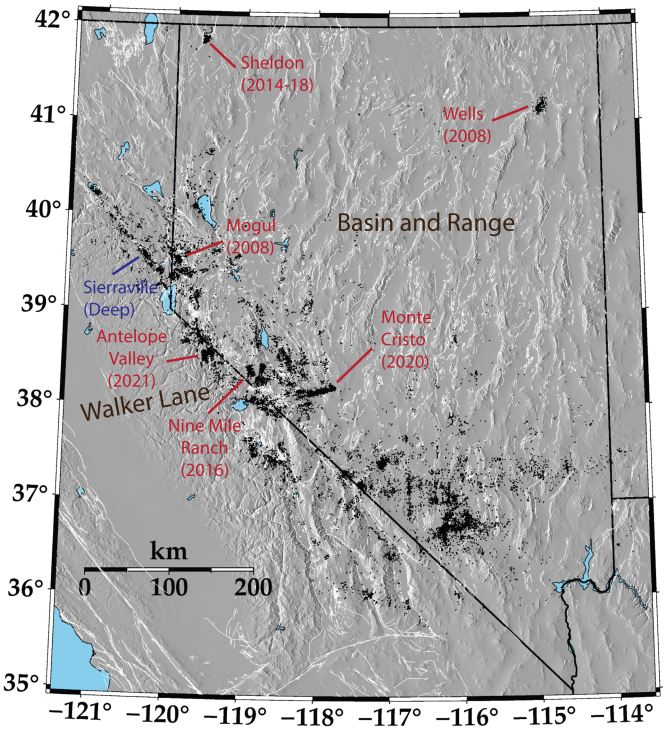

Figure 3. Relocated seismicity (black dots) in Nevada and the surrounding region, with select prominent sequences and tectonic regions annotated. The color version of this figure is available only in the electronic edition.

Downloaded from http://pubs.geoscienceworld.org/ssa/srl/article-pdf/doi/10.1785/0220240106/6527156/srl-2024106.1.pdf
by University of Nevada Reno, dtrugman

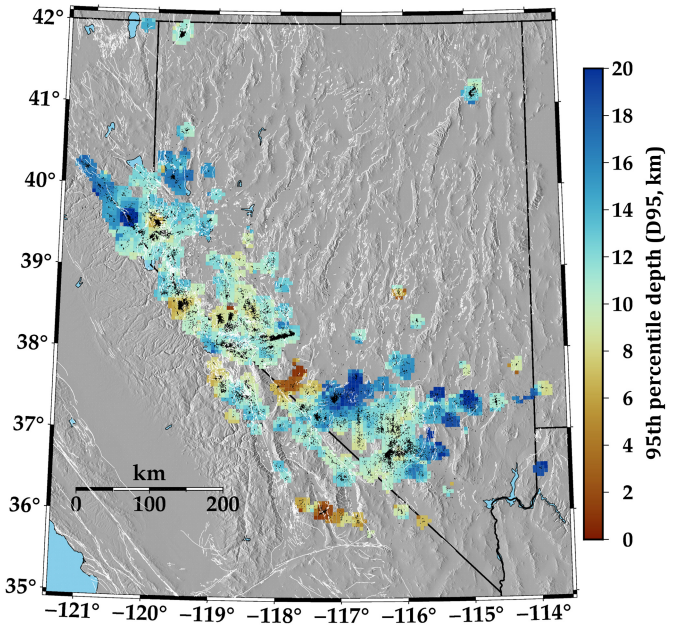

Figure 4. Depth distributions of seismicity displayed as 95th percentile depths of earthquakes aggregated in spatial grid cells of radius 10 km. Only cells with at least 30 events are displayed. The color version of this figure is available only in the electronic edition.

depth distribution of seismicity varies substantially across Nevada. The deepest events occur beneath the Sierra Nevada west of Reno as well as in portions of southeastern Nevada. A particularly intriguing sequence occurred beneath Sierraville in eastern California. These events, first discovered by Smith *et al.* (2016), occur on an east-dipping fault plane at ~35 km depth that is sharply imaged by the new catalog (Fig. 5) and may be a northern extension of similar seismicity clusters to the south, beneath Lake Tahoe (Smith, 2004). Clusters of shallow seismicity occur across Nevada, including near Mogul (a suburb of Reno), in the central and southern Walker Lane, and in southern Nevada within the NNSS. In the northern Walker Lane (except Mogul), events tend to be deeper than those to the south or in the Basin and Range.

In addition to these improvements to location accuracy and precision, the new catalog also provides revised local magnitude (M_L) estimates (Fig. 6a). The changes in magnitude estimates come primarily from the changes to the distance correction function at distances <20 km (which was previously saturated) and from the consideration of local site amplification effects. Although magnitude revisions for individual events can be significant, the median changes are in the 0.1–0.2 unit range and are typically positive for very small events and slightly negative for larger ones (Fig. 6b). Small earthquakes are typically recorded with good signal-to-noise only at the closest distances, which explains the observed tendency for larger and typically positive magnitude revisions for the smallest events. Events along the California–Nevada border often have alternate origins from the USGS or regional networks in California, and we can use the M_L values reported by other networks to confirm that our revised M_L values are well-calibrated (Fig. 6c).

From the curvature of the magnitude histogram, the completeness level for the catalog appears to be ~1.4, though this is not uniformly true for the duration of the catalog, particularly during active sequences like Monte Cristo where detailed cataloging of all events is not feasible. Using a more conservative estimate for the magnitude of completeness of 1.8, we obtain a *b*-value estimate of 0.84 using the maximum-likelihood approach (e.g., Bender, 1983), with uncertainties of ±0.02 units obtained through bootstrap resampling. This value is lower than the *b*-value estimates of 0.9–1.0 obtained from comparable catalogs in California (Hutton *et al.*, 2010), suggesting Nevada earthquake sequences tend to have relatively more frequent large events. The *b*-value estimate we report pertains to M_L and not moment magnitude M_w. A conversion to M_w for this purpose would increase the *b*-value estimate, though this would not explain the discrepancy with California networks, which also use M_L or M_D by default for small earthquakes.

Zaliapin *et al.* (2008) and Zaliapin and Ben-Zion (2013a,b) developed a rigorous methodology for analyzing the clustering statistics of earthquake sequences based on the nearest-neighbor analyses in the joint magnitude–distance–time space. We apply this technique to partition the Nevada catalog into individual earthquake sequences, using the *b*-value determined above and a threshold parameter determined by inspection of the bimodal nearest-neighbor diagram. We then isolate sequences with mainshock magnitude (M_L) greater than 4.0 and compute the sequence productivity factor defined by Trugman and Ben-Zion (2023), which quantifies the relative activity level of earthquake sequences, accounting for the expected trends with earthquake magnitude. Productivity defined in this way is measured on a $\log_{10}$ scale and is centered at zero, such that values of 0 correspond to typical levels of activity, whereas values of +1 and −1 correspond to levels of activity a factor of 10× greater or less than expected for a given mainshock magnitude. Displaying the sequence productivity factors in map view (Fig. 7), spatial patterns are readily discernible, with enhanced productivity observed throughout the central and northern Walker Lane. The most productive sequence is within the Sheldon Wildlife Refuge in the far northwest of the study region (Trugman, Savran *et al.*, 2023), whereas sequences in southern and eastern Nevada, as well as those beneath the Sierra, are less productive than average.

Discussion

The new, high-precision earthquake catalog developed through this study reveals interesting patterns in seismicity across the Walker Lane and Basin and Range. In particular, we observe

Downloaded from http://pubs.geoscienceworld.org/ssa/srl/article-pdf/doi/10.1785/0220240106/6527156/srl-2024106.1.pdf
by University of Nevada Reno, dtrugman

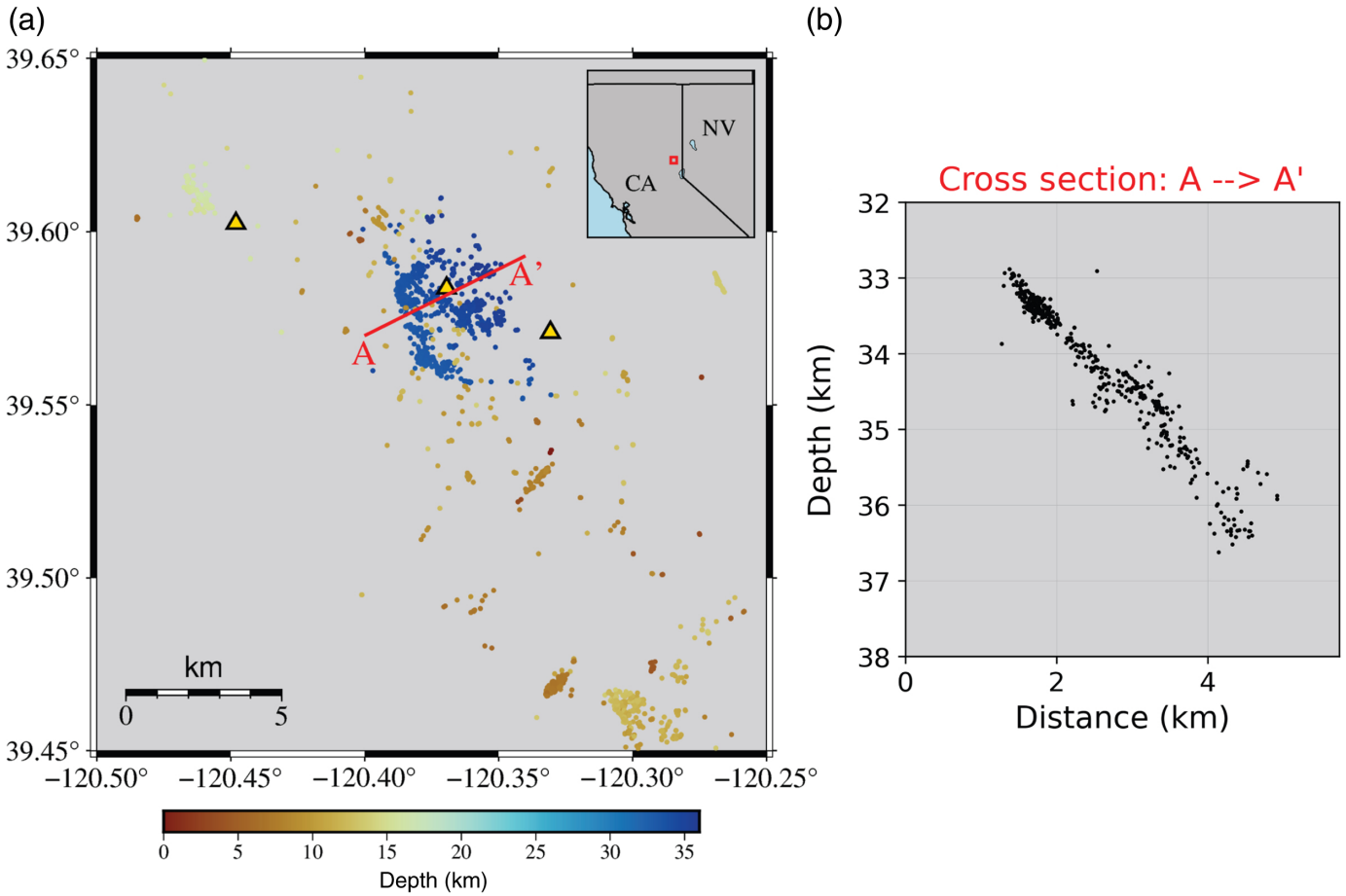

Figure 5. Deep earthquakes near Sierraville, California, displayed in (a) map view, color coded by depth with the study region shown in the inset and (b) cross section for the A–A′ line marked in panel (a). The color version of this figure is available only in the electronic edition.

coherent spatial variations in the depth distributions and clustering properties of earthquake sequences across the region. Although the variations appear systematic, the causes underlying them are not yet well understood. The D95 parameter is often used as a proxy for the depth of the seismogenic zone (Hauksson, 2011; Zeng *et al.*, 2022), but it seems unlikely (at least to this author) that the seismogenic thickness truly varies from as shallow as 4 km to as deep as 35 km over such short spatial scales (Fig. 4). Localized areas of elevated heat flow may compress the seismogenic thickness, but it seems likely that at least some of the observed variations in D95 arise due to the finite duration of the catalog. Averaged over geologic time, D95 may indeed closely correspond to seismogenic thickness, but there is no such guarantee over shorter timescales, for which seismicity statistics may be dominated by individual clusters. This effect is particularly pronounced for the new Nevada catalog, with a duration of only 16 yr, but may also be relevant for interpretations of other instrumental catalogs for which duration with adequate depth resolution is short compared to the recurrence intervals of large earthquakes.

Trugman and Ben-Zion (2023) observed that earthquake sequences in Walker Lane are more productive than their counterparts to the west along the plate boundary faults of California. Indeed, the earthquakes in this Nevada-centric catalog have distinct statistical properties compared to what is observed in California, with both lower *b*-values and a greater degree of clustering. The newly enhanced earthquake catalog permits us to study Nevada seismicity in greater detail, revealing for example the tendency for sequences in central and northern Walker Lane to be more productive than those further to the west in the Sierra proper or the east in Basin and Range (Fig. 7). The physical mechanisms underlying these spatial patterns require a more in-depth investigation; as noted by Trugman and Ben-Zion (2023), there are significant statistical relations between productivity, heat flow, and faulting complexity, but the exact causal nature of these relations remains uncertain. Similarly, the driving forces associated with anomalously deep earthquakes beneath Sierraville, California (Fig. 5), remain quite mysterious, but the precise locations of these events yielded by this study may help unlock the relevant physical processes in future research.

The main purpose of this article is to provide the scientific community with a research-quality earthquake catalog for the

Downloaded from http://pubs.geoscienceworld.org/ssa/srl/article-pdf/doi/10.1785/0220240106/6527156/srl-2024106.1.pdf
by University of Nevada Reno, dtrugman

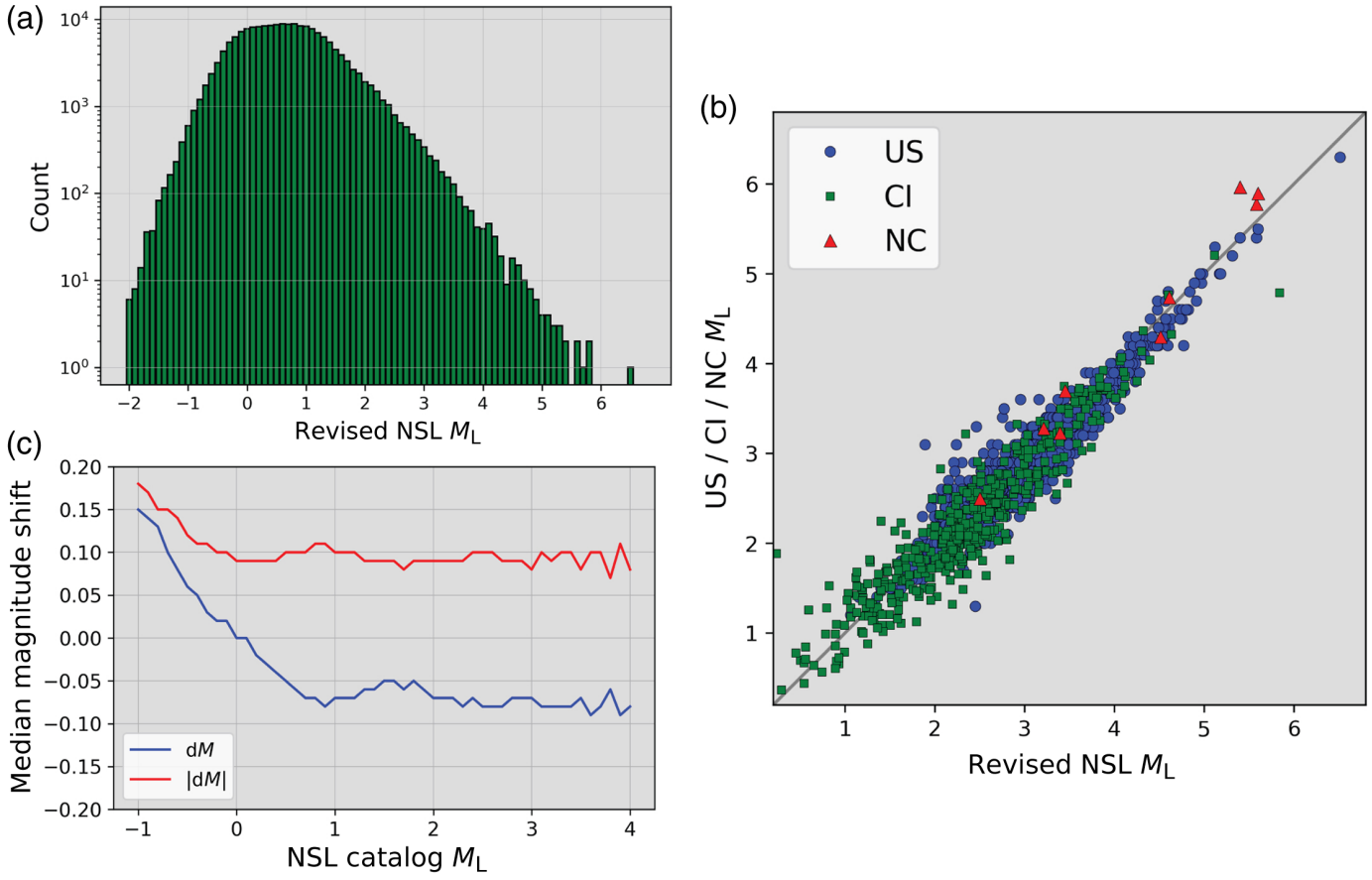

Figure 6. Magnitude statistics of the Nevada catalog. (a) Frequency–magnitude distribution for the revised local magnitude (M_L) scale proposed in this study. (b) Comparison of revised NSL magnitudes (*x* axis) with estimates from other ComCat magnitude sources (*y* axis). (c) Median shift in magnitude for earthquakes of different sizes, binned by original NSL catalog magnitude (*x* axis). The bottom and top curves correspond to signed and absolute shift values, respectively. CI, Southern California; NC, Northern California; US, USGS. The color version of this figure is available only in the electronic edition.

state of Nevada. Although the hope is that the catalog becomes widely used, users need to keep in mind its current limitations. The accuracy of earthquake locations is intrinsically tied to the fidelity of the velocity model; in this case, we use a new 3D model (Doody *et al.*, 2023) that is considered the best available for the region, but we cannot hope to resolve all fine-scale lateral and depth-dependent variations that could influence seismic arrival times. Through waveform cross-correlation and relative relocation, we can greatly enhance the location precision of a subset of the complete catalog. The relocated events are of great value in interpreting fault structures and the geometry of seismicity, but it is important to recognize that many of the largest events cannot be relocated in this way due to the complexity of their waveforms, precluding sufficient cross-correlation with neighboring events. Thus, when interpreting the time evolution, magnitude statistics, or moment release of the catalog, it is important to consider all events and not just those that are waveform relocated. Similarly, while the revised magnitude scale is an improvement over the current standard of practice at the NSL, the magnitude estimates are still fundamentally local magnitudes, which are instrumental measurements that do not always correspond directly to the size of the earthquake. Future work could be dedicated to the routine estimation of moment magnitudes and other source characteristics like focal mechanisms that would provide additional insight into earthquake processes in Nevada and beyond.

Data and Resources

Earthquake catalog and waveform data used in this study were obtained from Nevada Seismological Laboratory (NSL; http://www.seismo.unr.edu/Earthquake). Data processing was performed in Python and Julia, with geographic figures produced using PyGMT (https://www.pygmt.org/dev/overview.html). NonLinLoc (https://github.com/alomax/NonLinLoc) and GrowClust3D.jl (https://github.com/dttrugman/GrowClust3D.jl) are both open-science repositories. Statistical seismology functions use the public StatSei.jl repository available at https://github.com/dttrugman/StatSei.jl. Quaternary faults and fold data used for geographic visualization were obtained from the U.S. Geological Survey (USGS) database (https://www.sciencebase.gov/catalog/item/589097b1e4b072a7ac0cae23). The relocated earthquake catalog compiled in this study, along with the station terms associated with the revised local magnitude scale is

Downloaded from http://pubs.geoscienceworld.org/ssa/srl/article-pdf/doi/10.1785/0220240106/6527156/srl-2024106.1.pdf
by University of Nevada Reno, dtrugman

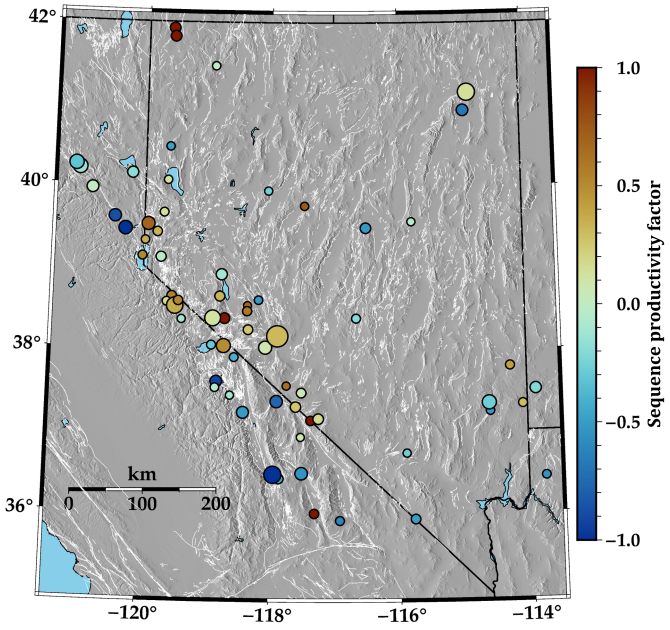

Figure 7. Spatial variations in the productivity of all earthquake sequences that include an M_L 4.0 or greater mainshock (largest event). Warmer and cooler colors (positive and negative productivity values) correspond to sequences that are more or less active than the dataset average. The size of the circle representing each sequence scales with mainshock magnitude. The color version of this figure is available only in the electronic edition.

archived on Zenodo (doi: 10.5281/zenodo.10698871). All websites were last accessed in May 2024.

Declaration of Competing Interests

The author acknowledges that there are no conflicts of interest recorded.

Acknowledgments

The study was supported by the National Aeronautics and Space Administration (NASA) Award Number 80NSSC24K0736, National Science Foundation (NSF) Award Numbers EAR-2121666 and EAR-2231705, and the Nevada Division of Emergency Management Award Number HMGP DR-4523-08-08P. The author thanks K. Bogolub and B. Savran for an internal review and useful suggestions to improve the article and associated catalog. The author also thanks R. Skoumal, an anonymous reviewer, and the associate editor for their constructive and timely feedback on the article.

References

Bender, B. (1983). Maximum likelihood estimation of b values for magnitude grouped data, *Bull. Seismol. Soc. Am.* **73,** no. 3, 831–851, doi: 10.1785/BSSA0730030831.

Doody, C., A. Rodgers, M. Afanasiev, C. Boehm, L. Krischer, A. Chiang, and N. Simmons (2023). CANVAS: An adjoint waveform tomography model of California and Nevada, *J. Geophys. Res.* **128,** no. 12, e2023JB027583, doi: 10.1029/2023JB027583.

Gianella, V. P., and E. Callaghan (1934). The Cedar Mountain, Nevada, earthquake of December 20, 1932, *Bull. Seismol. Soc. Am.* **24,** no. 4, 345–384, doi: 10.1785/BSSA0240040345.

Hatch-Ibarra, R. L., R. E. Abercrombie, C. J. Ruhl, K. D. Smith, W. C. Hammond, and I. K. Pierce (2022). The 2016 Nine Mile Ranch earthquakes: Hazard and tectonic implications of orthogonal conjugate faulting in the Walker Lane, *Bull. Seismol. Soc. Am.* **112,** no. 3, 1727–1741, doi: 10.1785/0120210149.

Hauksson, E. (2011). Crustal geophysics and seismicity in southern California, *Geophys. J. Int.* **186,** no. 1, 82–98, doi: 10.1111/j.1365-246X.2011.05042.x.

Hauksson, E., W. Yang, and P. M. Shearer (2012). Waveform relocated earthquake catalog for Southern California (1981 to June 2011), *Bull. Seismol. Soc. Am.* **102,** no. 5, 2239–2244, doi: 10.1785/0120120010.

Hutton, K., J. Woessner, and E. Hauksson (2010). Earthquake monitoring in Southern California for seventy-seven years (1932-2008), *Bull. Seismol. Soc. Am.* **100,** no. 2, 423–446, doi: 10.1785/0120090130.

Jennings, P. C., and H. Kanamori (1983). Effect of distance on local magnitudes found from strong-motion records, *Bull. Seismol. Soc. Am.* **73,** no. 1, 265–280, doi: 10.1785/BSSA0730010265.

Jones, J. C. (1915). The pleasant valley, Nevada, earthquake of October 2, 1915, *Bull. Seismol. Soc. Am.* **5,** no. 4, 190–205, doi: 10.1785/BSSA0050040190.

Lomax, A., A. Michelini, and A. Curtis (2014). Earthquake location, direct, global-search methods, in *Encyclopedia of Complexity and Systems Science*,R. A. Meyers (Editor), Springer, New York, New York, 1–33, doi: 10.1007/978-3-642-27737-5_150-2.

Lomax, A., J. Virieux, P. Volant, and C. Berge-Thierry (2000). Probabilistic earthquake location in 3D and layered models, in *Advances in Seismic Event Location*,C. H. Thurber and N. Rabinowitz (Editors), Modern Approaches in Geophysics, Springer, Dordrecht, The Netherlands, 101–134, doi: 10.1007/978-94-015-9536-0_5.

Mendoza, C., and S. Hartzell (2009). Source analysis using regional empirical Green's functions: The 2008 Wells, Nevada, earthquake, *Geophys. Res. Lett.* **36,** no. 11, doi: 10.1029/2009GL038073.

Richter, C. F. (1935). An instrumental earthquake magnitude scale, *Bull. Seismol. Soc. Am.* **25,** no. 1, 1–32.

Richter, C. F. (1958). *Elementary Seismology*, W. H. Freeman, San Francisco, California.

Ruhl, C. J., R. E. Abercrombie, K. D. Smith, and I. Zaliapin (2016). Complex spatiotemporal evolution of the 2008 Mw 4.9 Mogul earthquake swarm (Reno, Nevada): Interplay of fluid and faulting, *J. Geophys. Res.* doi: 10.1002/2016JB013399.

Ruhl, C. J., E. A. Morton, J. M. Bormann, R. Hatch-Ibarra, G. Ichinose, and K. D. Smith (2021). Complex fault geometry of the 2020 Mww 6.5 Monte Cristo Range, Nevada, earthquake sequence, *Seismol. Res. Lett.* **92,** no. 3, 1876–1890, doi: 10.1785/0220200345.

Ryall, A. (1977). Earthquake hazard in the Nevada region, *Bull. Seismol. Soc. Am.* **67,** no. 2, 517–532, doi: 10.1785/BSSA0670020517.

Slemmons, D. B. (1957). Geological effects of the Dixie Valley-Fairview Peak, Nevada, earthquakes of December 16, 1954, *Bull. Seismol. Soc. Am.* **47,** no. 4, 353–375, doi: 10.1785/BSSA0470040353.

Downloaded from http://pubs.geoscienceworld.org/ssa/srl/article-pdf/doi/10.1785/0220240106/6527156/srl-2024106.1.pdf
by University of Nevada Reno, dtrugman

Smith, K. D. (2004). Evidence for deep magma injection beneath Lake Tahoe, Nevada-California, *Science* **305,** no. 5688, 1277–1280, doi: 10.1126/science.1101304.

Smith, K. D., G. M. Kent, D. P. von Seggern, N. W. Driscoll, and A. Eisses (2016). Evidence for Moho-lower crustal transition depth diking and rifting of the Sierra Nevada microplate, *Geophys. Res. Lett.* **43,** no. 20, 10,738–10,744, doi: 10.1002/2016GL070283.

Tocher, D. (1956). Movement on the Rainbow Mountain fault, *Bull. Seismol. Soc. Am.* **46,** no. 1, 10–14, doi: 10.1785/BSSA0460010010.

Trugman, D. T., and Y. Ben-Zion (2023). Coherent spatial variations in the productivity of earthquake sequences in California and Nevada, *Seism. Record* **3,** no. 4, 322–331, doi: 10.1785/0320230039.

Trugman, D. T., and P. M. Shearer (2017). GrowClust: A hierarchical clustering algorithm for relative earthquake relocation, with application to the Spanish springs and Sheldon, Nevada, earthquake sequences, *Seismol. Res. Lett.* **88,** no. 2A, 379–391, doi: 10.1785/0220160188.

Trugman, D. T., J. Brune, K. D. Smith, J. N. Louie, and G. M. Kent (2023). The rocks that did not fall: A multidisciplinary analysis of near-source ground motions from an active normal fault, *AGU Adv.* **4,** no. 2, e2023AV000885, doi: 10.1029/2023AV000885.

Trugman, D. T., C. J. Chamberlain, A. Savvaidis, and A. Lomax (2022). GrowClust3D.jl: A Julia package for the relative relocation of earthquake hypocenters using 3D velocity models, *Seismol. Res. Lett.* **94,** no. 1, 443–456, doi: 10.1785/0220220193.

Trugman, D. T., W. H. Savran, C. R. Ruhl, and K. D. Smith (2023). Unraveling the evolution of an unusually active earthquake sequence Near Sheldon, Nevada, *Seismica* **2,** no. 2, doi: 10.26443/seismica.v2i2.1051.

Uhrhammer, R. A., M. Hellweg, K. Hutton, P. Lombard, A. W. Walters, E. Hauksson, and D. Oppenheimer (2011). California integrated seismic network (CISN) local magnitude determination in California and vicinity, *Bull. Seismol. Soc. Am.* **101,** no. 6, 2685–2693, doi: 10.1785/0120100106.

Waldhauser, F., and W. L. Ellsworth (2000). A double-difference earthquake location algorithm: Method and application to the Northern Hayward Fault, California, *Bull. Seismol. Soc. Am.* **90,** no. 6, 1353–1368, doi: 10.1785/0120000006.

Waldhauser, F., and D. P. Schaff (2008). Large-scale relocation of two decades of Northern California seismicity using cross-correlation and double-difference methods, *J. Geophys. Res.* **113,** no. B8, doi: 10.1029/2007JB005479.

Zaliapin, I., and Y. Ben-Zion (2013a). Earthquake clusters in southern California I: Identification and stability, *J. Geophys. Res.* **118,** no. 6, 2847–2864, doi: 10.1002/jgrb.50179.

Zaliapin, I., and Y. Ben-Zion (2013b). Earthquake clusters in southern California II: Classification and relation to physical properties of the crust, *J. Geophys. Res.* **118,** no. 6, 2865–2877, doi: 10.1002/jgrb.50178.

Zaliapin, I., A. Gabrielov, V. Keilis-Borok, and H. Wong (2008). Clustering analysis of seismicity and aftershock identification, *Phys. Rev. Lett.* **101,** no. 1, 018501, doi: 10.1103/PhysRevLett.101.018501.

Zeng, Y., M. Petersen, and O. Boyd (2022). Lower Seismogenic depth model for Western U.S. earthquakes, *Seismol. Res. Lett.* **93,** no. 6, 3186–3204, doi: 10.1785/0220220174.

Manuscript received 18 March 2024
Published online 24 June 2024

Downloaded from http://pubs.geoscienceworld.org/ssa/srl/article-pdf/doi/10.1785/0220240106/6527156/srl-2024106.1.pdf
by University of Nevada Reno, dtrugman